Recent Warming and Freshening of the Norwegian Sea Observed by Argo Data

KJELL ARNE MORK, ØYSTEIN SKAGSETH, AND HENRIK SØILAND

Institute of Marine Research and Bjerknes Centre for Climate Research, Nordnes, Bergen, Norway

(Manuscript received 10 September 2018, in final form 18 March 2019)

ABSTRACT

Climate variability in the Norwegian Sea, comprising the Norwegian and Lofoten Basins, was investigated based upon monthly estimates of ocean heat and freshwater contents using data from Argo floats during 2002–18. Both local air–sea exchange and advective processes were examined and quantified for monthly to interannual time scales. In the recent years, 2011–18, the Norwegian Sea experienced a decoupling of the temperature and salinity, with a simultaneous warming and freshening trend. This was mainly explained by two different processes; reduced ocean heat loss to the atmosphere and advection of fresher Atlantic water into the Norwegian Sea. The local air–sea heat fluxes are important in modifying the ocean heat content, although this relationship varied with time scale and basins. On time scales exceeding 4 months in the Lofoten Basin and 6 months in the Norwegian Basin, the air–sea heat flux explained half or even more of the local ocean heat content change. There were both a short-term and long-term response of the wind forcing on the ocean heat content. The monthly to seasonal response of increased southerly wind cooled and freshened the Norwegian Basin, due to eastward surface Ekman transport, and increased the influence of Arctic Water. However, after about a 1-yr delay the ocean warmed and became saltier due to an increased advection of Atlantic Water into the region. Increased westerly winds decreased the ocean heat content in both cases due to increased transport of Arctic Water into the Norwegian Sea.

1. Introduction

Ecosystem changes in the Nordic seas (the Norwegian, Greenland, and Iceland Seas) are closely connected to the variability in the hydrographic conditions (Skjoldal 2004). The origin of this variability is connected to upstream circulation changes, such as in the subpolar gyre (Häkkinen and Rhines 2004) or in the North Atlantic ''inter-gyre gyre'' region (Marshall et al. 2001), generating anomalies that subsequently propagate along with the ocean circulation into the Nordic seas (Hatun et al. 2005) and northward (e.g., Holliday et al. 2008; Walczowski et al. 2012). Based on this, there is potential for predictability of hydrographic changes in the Nordic seas (Arthun et al. 2017; Langehaug et al. 2017). In this study, we quantified the changes in ocean heat and freshwater content at monthly scales in order to resolve the mechanism driving the observed hydrographic variability in the Nordic seas.

The Nordic seas together with the Labrador and Irminger Seas are major regions of water mass transformation in the northern loop of the global thermohaline circulation (e.g., Pickart and Spall 2007; Swift 1984; Vage et al. 2011). Atlantic Water (AW) is transformed, through intense cooling, into a water mass that is dense enough to feed the lower North Atlantic Deep Water (Aagaard et al. 1985). In the Nordic seas, this cooling occurs largely in the eastern region, that is, the Norwegian Sea (Eldevik et al. 2009; Isachsen et al. 2007; Segtnan et al. 2011). The inflow of AW to the Norwegian Sea occurs mainly between Iceland and Shetland (Fig. 1). On the western margin of the Nordic seas, cold and less saline Arctic water flows southward with the East Greenland Current (EGC). Most of this water enters the western North Atlantic, but a fraction flows directly into the Norwegian Sea as

Denotes content that is immediately available upon publication as open access.

Supplemental information related to this paper is available at the Journals Online website: https://doi.org/10.1175/JCLI-D-18-0591.s1.

Corresponding author: Kjell Arne Mork, kjell.arne.mork@hi.no

DOI: 10.1175/JCLI-D-18-0591.1

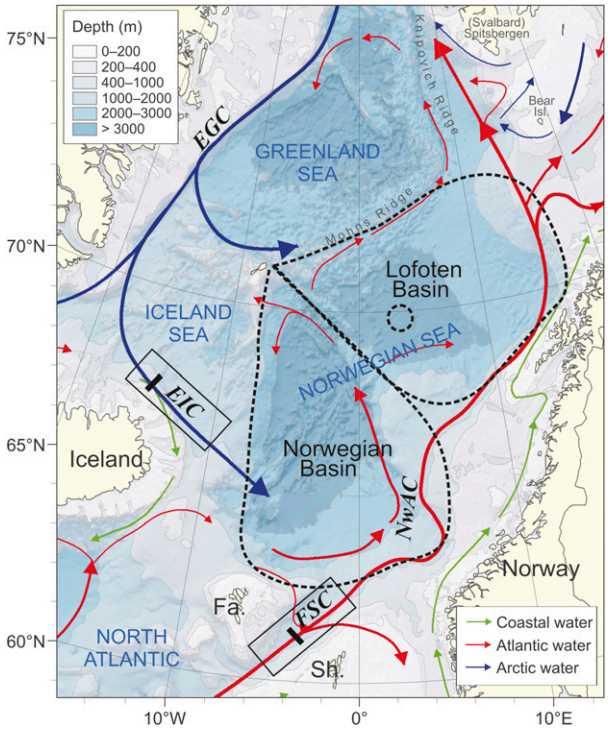

FIG. 1. Schematic view of the surface circulation in the Nordic seas. Red and blue vectors indicate warm, saline Atlantic Water and cold, fresh Arctic Water, respectively. NwAC = Norwegian Atlantic Current, EGC = East Greenland Current. The two study areas, the Lofoten and Norwegian Basins, are marked with dashed contours. The upstream areas are the East Icelandic Current (EIC) and Faroe–Shetland Channel (FSC) with wind time series (averaged over the boxes). The thick black lines at the upstream areas indicate where hydrographic time series exist (e.g., Hughes et al. 2011). The location of the Lofoten Basin eddy is marked with a black dashed circle in the Lofoten Basin.

the East Icelandic Current (EIC). The variability in the strength of these currents and their properties is essential for modifying the structure and distribution of the water masses in the Norwegian Sea (Blindheim et al. 2000).

The role of local air–ocean exchange in modifying the hydrographic anomalies is not clear from previous work. Carton et al. (2011) found no clear influence of local air–sea fluxes; in line with this, Arthun and Eldevik (2016), based on model analysis, reported anomalies propagating with minor dampening along-stream in the North Atlantic Current and its northward extension to the Fram Strait. Contradicting this view of minor modification, Mork et al. (2014) found that local air–sea heat fluxes account for about half of the interannual variation in the heat content of Atlantic water in the Nordic seas. Despite the potential important role of hydrographic anomalies in terms of prediction of hydrographic changes, the question regarding if and how, and the time scales over which, these anomalies are preserved and/or modified, remains open.

Here, we showed that by utilizing Argo data, it was possible to capture the heat and freshwater variability in the Norwegian Sea on time scales down to seasonally with reasonable accuracy. We used these to investigate the role of local air–sea exchange and advection on seasonal and interannual times scales on the hydrographic variability in the Norwegian Sea. We especially examined the period 2011–18 when the upper 1000 m in the Norwegian Sea became simultaneously warmer and fresher. This has, to our knowledge, not been reported by others.

2. Data and methods

The heat and freshwater contents were calculated from Argo data obtained from the Coriolis Global Data Assembly Centre (http://www.coriolis.eu.org/). Only delayed mode quality-controlled data with quality flagged good or changed were used (Carval et al. 2015). Argo data in the Norwegian Sea exist from 2002. Figure S1 in the online supplemental material shows the number of profiles in the Norwegian and Lofoten Basin each month from 2002 to mid-2018, and the analysis was performed separately for the two basins (Fig. 1). For the Norwegian Basin, the analysis was done for the period 2002–18. Given the limited number of profiles in the Lofoten Basin, the analysis was restricted to the period 2005–18 when existing data were sufficient for reliable estimates. About 10 profiles per month resolved the heat and freshwater content estimates on the seasonal scale. The number of profiles per month ranged from about 10 to 60 (Fig. S1).

The anomalies of the heat and freshwater contents were calculated relative to the *World Ocean Atlas 2018* (*WOA18*) climatology using the latest average period, 2005–17, which includes the coverage of Argo floats from 2005 (Locarnini et al. 2019; Zweng et al. 2018). The climatology consists of long-term monthly means of temperature T_{clim} and salinity S_{clim} on 0.25° grids. For each Argo profile, the temperature and salinity climatology were interpolated horizontally and vertically to match the location and vertical resolution of the Argo profile. The advantages of using anomalies are that they are independent of the reference value and less influenced by the location (i.e., less spatially biased). For each Argo profile, anomalies of the heat H and freshwater F contents, relative to the climatology, were calculated above the reference depth h

$$H' = H - H_{\text{clim}} = c_p \rho_0 \int_{-h}^{0} (T - T_{\text{clim}}) dz (\text{Jm}^{-2}), \quad (1)$$

$$F' = F - F_{\text{clim}} = -S_{\text{ref}}^{-1}\int_{-h}^{0}(S - S_{\text{clim}})\,dz(\text{m}), \qquad (2)$$

where c_p is the heat capacity ($4.2 \times 10^3\,\text{J}\,\text{kg}^{-1}\,\text{K}^{-1}$), ρ_0 is a reference density ($1030\,\text{kg}\,\text{m}^{-3}$), S_{ref} is a reference salinity (35 psu), and z is the vertical axis with $z = 0$ at the sea surface. Subscript "clim" indicates climatological data from *WOA18*. The terms H' and F' were calculated for $h = 200\,\text{m}$ and $h = 1000\,\text{m}$ where the former reference depth was chosen to represent the upper layer. The latter reference depth was a compromise between the coverage of the entire Atlantic layer in the Norwegian Sea and the number of sufficient deep vertical profiles. A particular feature in the Lofoten Basin is the Lofoten Basin eddy (LBE; e.g., Søiland and Rossby 2013), an anticyclonic permanent eddy with a 1000–1200-m-deep core of AW and radial distance of 15–20 km (see Fig. 1 for location). Since the hydrography in the LBE is distinct from the Lofoten Basin, the profiles within the LBE were omitted in the analysis. This was done by removing all profiles with temperatures, averaged between 900- and 1000-m depth, above 2.5°C (Bosse et al. 2018). The heat and freshwater content anomalies at each single location were used to calculate monthly averages with standard errors for both the Norwegian and Lofoten Basins, and hereafter used in all analyses.

The net air–sea heat fluxes (sum of radiative and turbulent fluxes) from the ERA-Interim dataset (Dee et al. 2011), produced by the European Centre for Medium-Range Weather Forecasts (ECMWF), were compared and correlated with the ocean heat content change. The significance (p value) of the correlations were evaluated by a Monte Carlo approach; running the correlation analysis 10 000 times with synthetic series that had similar autocorrelation properties as the air–sea heat fluxes. The relation between the ocean heat content change in the upper 200 m and the air–sea heat flux in the frequency domain was investigated by coherence analysis (e.g., Emery and Thompson 1997) applying the multitaper method (averaging over eight windows; Thomson 1982).

The net air–sea heat flux from the National Centers for Environmental Prediction and National Center for Atmospheric Research reanalysis (NCEP; Kalnay et al. 1996) was compared with both the ERA-Interim air–sea heat flux and the ocean heat content change to assess if the analysis was sensitive to the reanalysis product.

An attempt was made to obtain qualitative relationships between advection of Atlantic and Arctic waters with hydrographic changes in the Norwegian Sea using local wind components from the ERA-Interim dataset as proxies for the variability of the current through the Faroe-Shetland Channel (FSC) and the EIC (see Fig. 1 for locations). Sherwin et al. (2008) combined hydrographic and acoustic Doppler current profiler data from 1994 to 2005 to estimate the northeastward transport through the FSC and to determine the monthly variability in the transport. They concluded that the seasonal variations in the transport appear to correlate with the local southwest wind stress, which may contribute to nearly half of the long-term transport in the channel. The dominant periods of the shelf edge current extending from the Irish–Scottish shelf to the Arctic Ocean are 2–30 days, which appears to be an indirect response to local winds or free waves (Gordon and Huthnance 1987; Skagseth and Orvik 2002) as wind modulates the sea level in the along-stream direction of the shelf edge current on monthly to annual time scales (Skagseth 2004; Skagseth et al. 2004). Compared to the current through the FSC, there exists little knowledge about the long-term variability of the EIC and its relationships with the wind forcing. Most recent, Macrander et al. (2014) did not find any relation to the large-scale atmospheric forcing, but instead found that the strength of the EIC was correlated with the local wind stress. We acknowledge that this relation is relatively weak, but still think that a wind-derived proxy for the EIC can be useful.

Changes in ocean heat content within a basin are induced by local air–sea heat fluxes and advective and diffusive heat transports through the basin boundaries (Moisan and Niiler 1998):

$$\underbrace{\frac{\partial \hat{H}'}{\partial t} - \hat{Q}'_{\text{net}}}_{\text{local change}} = Q'_{\text{res}}. \qquad (3)$$

Here Q_{net} is the local net air–sea heat flux, and Q_{res} represents the sum of advective and diffusive heat transports through the basin boundaries and balances the residual local heat content change in the basin. In this study, we set the vertical advection and horizontal diffusion heat transports to zero. Since the focus was on the temporal variability, we considered the vertical advection to have minor impact on the results. The prime indicates the anomaly relative to the long-term mean while the hat indicates basin-averaged values. We investigated the role of two main advective upstream sources on changes in the local heat and freshwater content in the upper 200 and 1000 m. This was done using the proxies of the current strength at the main upstream sources of AW at the FSC and of Arctic water in the EIC, as described previously, where information about the hydrographic variability and transport estimates exist (see Fig. 1 for locations; e.g., Hughes et al. 2011). The residual local heat content change was correlated

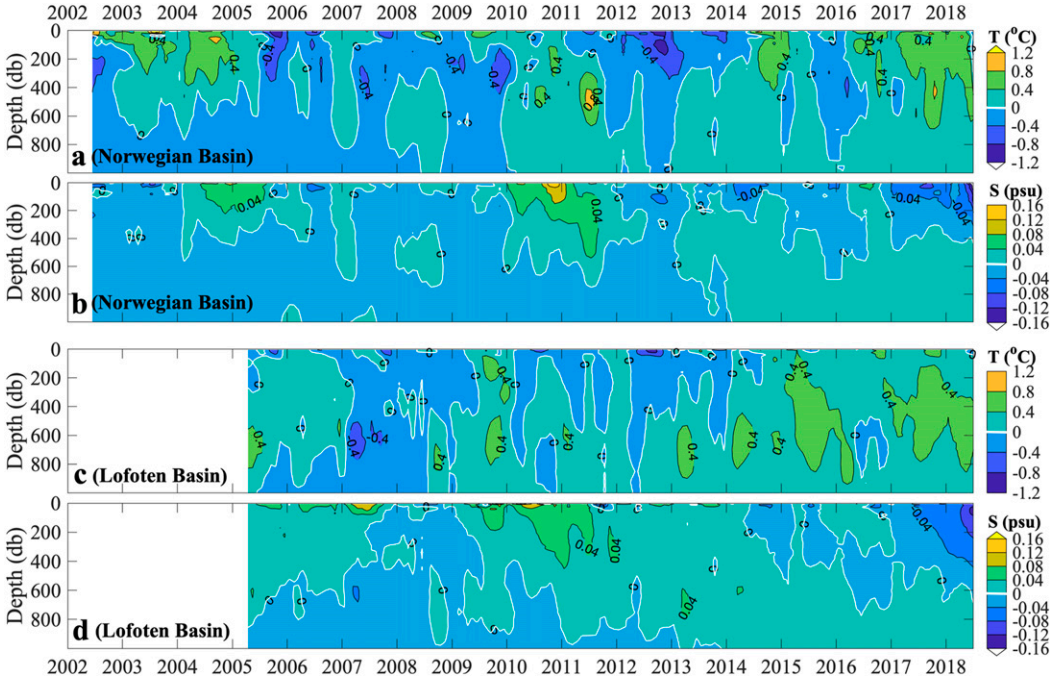

FIG. 2. (a),(c) Temperature and (b),(d) salinity anomalies, relative to *WOA18*, in the Norwegian Basin in (a) and (b) and the Lofoten Basin in (c) and (d). All data were smoothed using moving averages with a 3-month boxcar filter.

with the current strength proxies. The significance (p value) of the correlations was evaluated by a Monte Carlo approach similar to that described previously: using synthetic series that had autocorrelation properties similar to the wind-derived proxies. The analysis was performed twice on each dataset where the time series in advance were low-pass filtered using 3- or 12-month boxcar windows moving averages. The 3- and 12-month averages represent the variability on seasonal and interannual time scales, respectively. Correlation analysis using time lags from 0 to 18 months between the wind-derived proxies and the residual HCA was also carried out. A period of 18 months corresponds roughly to the time for anomalies to propagate from the FSC and into the Norwegian Sea (e.g., Chafik et al. 2015; Holliday et al. 2008). Similar correlation analysis was also performed for the freshwater content change.

3. Results

Time series of monthly averages of temperature and salinity anomalies in the upper 1000 m revealed variability on seasonal time scales (Fig. 2). In general, the variability extended deeper in the Lofoten Basin compared to the Norwegian Basin (e.g., the positive temperature anomalies). The timing of low and high temperature anomalies seemed to occur differently for the two basins, except for the last years when a warming and freshening occurred in both basins. The warming appeared in the whole 1000-m layer while the freshening happened only in the upper half of the layer considered here.

Time series of the heat and freshwater content anomalies (HCA and FwCA, respectively) reveal interannual and longer time scales overlying the seasonal variability (Fig. 3). Whereas high HCA values were observed for both basins in recent years (after 2013), the lowest FwCA (highest salinities) were in 2010–11 for both basins. Afterward, both basins experienced notable changes with simultaneously warming and freshening trends in the upper 1000 m (Table 1). All trends were 95% significant and about similar for the two basins; HCA in the Norwegian Basin, $0.20 \pm 0.05\ 10^9\ \mathrm{J\,m^{-2}\,yr^{-1}}$ and in the Lofoten Basin, $0.25 \pm 0.04\ 10^9\ \mathrm{J\,m^{-2}\,yr^{-1}}$. For the 2011–18 period, this corresponded to 6.3 ± 1.6 and $7.9 \pm 1.3\ \mathrm{W\,m^{-2}}$ for the Norwegian and Lofoten Basins, respectively (Table 1). For the FwCA, the trend was about twice as large in the Lofoten Basin compared to the Norwegian Basin, 0.14 ± 0.02 versus $0.06 \pm 0.02\ \mathrm{m\,yr^{-1}}$. Over the 2011–18 period, this corresponded to respectively a 1.1- and 0.5-m freshwater content increase. The corresponding trends for the temperature and salinity anomalies in the upper 1000 m were $0.046°\mathrm{C\,yr^{-1}}$

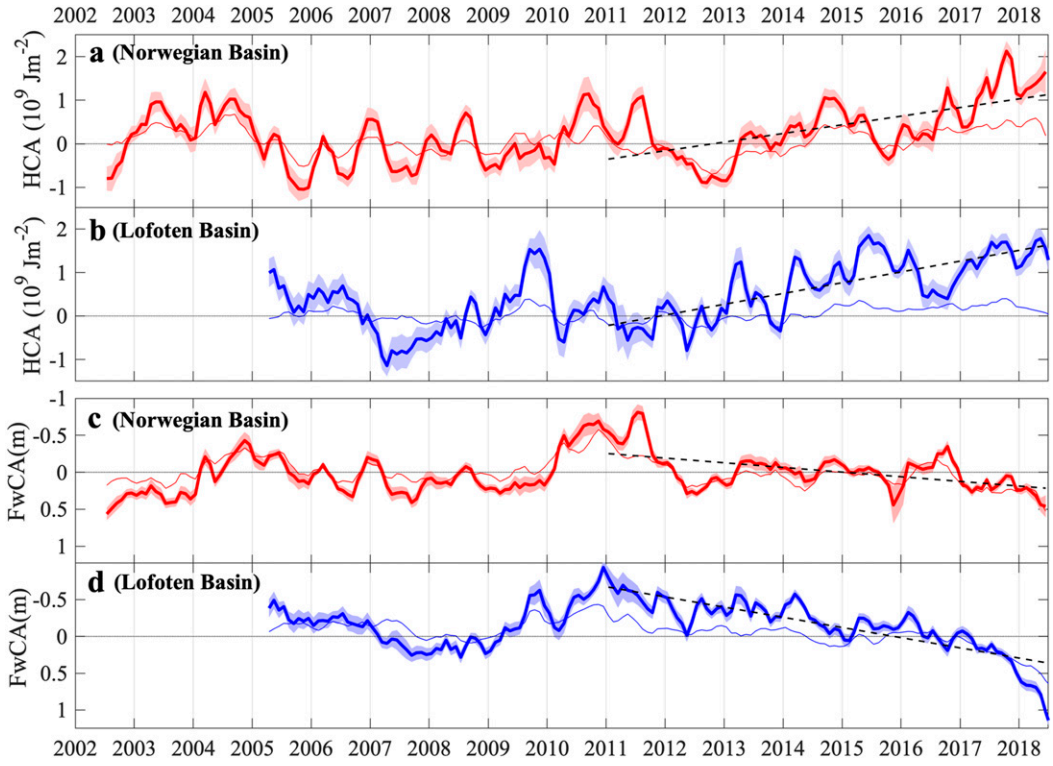

FIG. 3. Time series of heat content anomaly H' (0–1000 dbar) with standard error (shaded area) for both the (a) Norwegian and (b) Lofoten Basins. The thin lines are H' (0–200 dbar). All time series are filtered with 3-month running averages using a boxcar filter. (c),(d) As in (a) and (b), but for the freshwater content anomaly. The y axis is reversed. The trends for H' (0–1000 dbar) and F' (0–1000 dbar) over 2011–18 are indicated as dashed lines.

and -0.0024 psu yr^{-1} for the Norwegian Basin, and 0.051°C yr^{-1} and -0.0051 psu yr^{-1} for the Lofoten Basin. Thus, during 2011–18, in the upper 1000 m, the Norwegian and Lofoten Basins warmed 0.35° and 0.39°C, respectively, and freshened 0.018 and 0.039 psu, respectively. The variability in HCA and FwCA were primarily in the upper 200 m for the Norwegian Basin, but in the Lofoten Basin the main contribution was below 200 m.

Considering the upper 200 m, the HCA changes had larger variability in the Norwegian Basin compared to both the Lofoten Basin and the net local air–sea heat fluxes (Figs. 4a,b). The wind component at FSC and EIC had about the same level of variability (Fig. 4c). The NCEP net air–sea heat flux anomalies were also plotted for comparison with the ERA data, and show similar variation (Figs. 4a,b). Using monthly values, the correlation coefficient r between the HCA changes and air–sea heat flux anomalies for both the Norwegian Basin ($r = 0.25$) and Lofoten Basin ($r = 0.35$) were low but still significant at 95%. Using the NCEP data, the correlation analysis gave nearly the same correlation coefficients, $r = 0.25$ and $r = 0.34$, for the Norwegian and Lofoten Basins, respectively.

The relationship between the HCA change and air–sea heat fluxes was frequency dependent. On time scales longer than 6 months, the squared coherence between the air–sea heat flux and the HCA change was above the 95% confidence level in both basins (Fig. 5). At these time scales, the phase was also stable and near zero,

TABLE 1. Trends with the 95% confidence interval of heat content, freshwater content, temperature, and salinity anomalies in the upper 1000 m during 2011–18, for the Norwegian Basin (NB) and Lofoten Basin (LB). The numbers in parentheses for temperature and salinity are the changes during 2011–18.

	HCA	FwCA	Temperature	Salinity
NB	6.3 ± 1.6 W m^{-2}	0.06 ± 0.02 m yr^{-1}	0.046° ± 0.035°C yr^{-1} (2011–18: 0.35°C)	−0.0024 ± 0.0018 psu yr^{-1} (2011–18: −0.018 psu)
LB	7.9 ± 1.3 W m^{-2}	0.14 ± 0.02 m yr^{-1}	0.051° ± 0.031°C yr^{-1} (2011–18: 0.39°C)	−0.0051 ± 0.0017 psu yr^{-1} (2011–18: −0.039 psu)

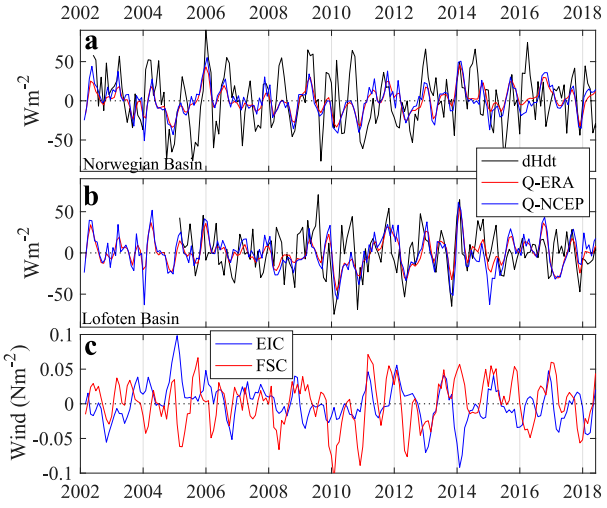

FIG. 4. Time series of monthly heat content anomaly (0–200 m) changes $dHdt$ and air–sea heat flux anomaly Q_{net} from the ERA-Interim and NCEP datasets for the (a) Norwegian and (b) Lofoten Basins. Negative values indicate ocean heat loss. (c) Time series of the wind-derived proxies at EIC and FSC. All time series are 3-month running averages using a 3-point boxcar filter of monthly values.

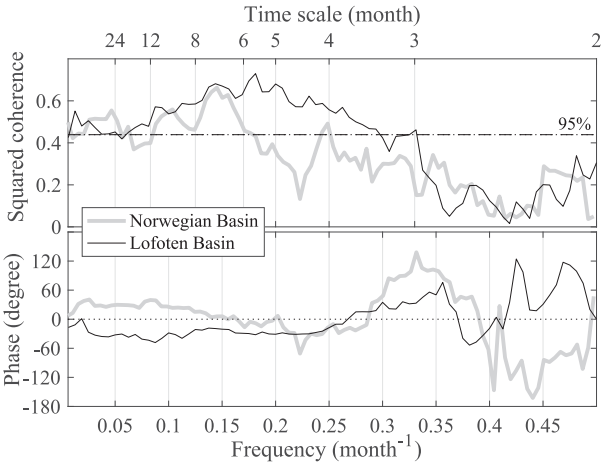

FIG. 5. Coherence analysis between heat content change $dH'dt$ in the upper 200 m and air–sea heat flux anomaly Q'_{net} for the Norwegian and Lofoten Basins. Monthly values are used in the analysis. The dashed line in the coherence plot is the 95% significance level. Positive phase indicates that Q'_{net} leads over the $dH'dt$. The lower and upper x axes are applicable to both the top and bottom panel.

implying no or little delay between the HCA changes and the air–sea heat fluxes. On 6-month and longer time scales, the squared coherence in the Norwegian Basin was above 0.5. In the Lofoten Basin, the coherence was also relatively high at periods from 4 months and longer with maximum coherence of 0.7 at 5–6 months. Using the HCA change in the upper 1000 m instead of that in the upper 200 m gave somewhat lower coherence in both basins, but the coherence was still 95% significant at time scales of about 1 year and 4–12 months in the Norwegian and Lofoten Basins, respectively.

To assess the role of advection on the residual HCA—that is, the part not explained by air–sea fluxes [see Eq. (3)]—and on the FwCA, correlation analysis was applied. The wind-derived proxies that qualitatively represent the variability of the EIC and the FSC (Fig. 4c) were correlated with the residual HCA change (Table 2). The wind component along the EIC was negatively correlated with the residual HCA change in the Norwegian Basin ($-0.4 < r < -0.2$), thus, implying that stronger EIC gives larger inflow of cold water. This held for HCA in the upper 200 and 1000 m. In the Lofoten Basin the wind at EIC was also negatively correlated with the residual HCA change in the upper 1000 m.

The wind component in the FSC was also negatively correlated with the residual HCA change in the Norwegian Basin for the upper 200 m ($-0.54 < r < -0.35$) and upper 1000 m for 12-month averages ($r = -0.38$; Table 2). A stronger inflow thus reduced the HCA. For the Lofoten Basin, the wind at the FSC was not significantly correlated with the residual HCA change.

Using time lags from 0 to 18 months between the wind at the FSC and the residual HCA for the upper 200 m showed that the correlations went from negative to positive for both the Norwegian and Lofoten Basins (Figs. 6a,b), but were only significant for the Norwegian Basin. At about 1-yr lag, the correlation coefficient for the Norwegian Basin was $r = 0.35$. The correlation between the wind at EIC and the residual HCA was negative for both basins at all time lags. Stronger westerly winds thus cooled both basins.

A similar correlation analysis, performed with the FwCA change, provided about similar correlation as the residual HCA change in the Norwegian Basin but with

TABLE 2. Correlation coefficients between the residual heat content change ($dHdt - Q$) and the wind-derived proxies at EIC and FSC. Two different lengths of moving averages are performed prior to the correlation, 3 and 12 months. Time resolution is 1 month in both cases. Correlation coefficients with 95% or higher significance are in bold.

		Norwegian Basin		Lofoten Basin	
Wind index	Avg length	200 m	1000 m	200 m	1000 m
EIC	3 months	**−0.22**	**−0.29**	−0.15	**−0.23**
	12 months	**−0.25**	**−0.37**	−0.11	**−0.20**
FSC	3 months	**−0.35**	−0.06	0.05	+0.15
	12 months	**−0.54**	**−0.38**	−0.13	+0.13

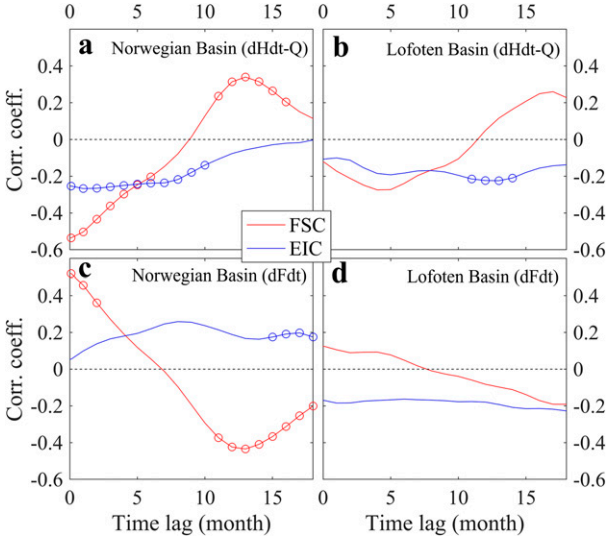

FIG. 6. Correlation coefficient between the residual heat content anomaly ($dHdt - Q$) change in the upper 200 m and the wind-derived proxies at EIC and FSC in the (a) Norwegian and (b) Lofoten Basins. The correlation coefficient is a function of time lag in months where wind is leading. Circles indicate correlation coefficients that are 95% significant. The 12-month moving averages using a boxcar filter were performed on the time series prior the analysis. (c),(d) As in (a) and (b), but using the freshwater content anomaly change $dFdt$ instead of the residual heat content change in the correlation analysis.

opposite sign (Figs. 6c,d). Thus, with no or little time lag, increased northerly wind through the FSC resulted in colder and fresher water in the Norwegian Basin, whereas after about a 1-yr lag the basin became warmer and saltier. Increased wind at EIC freshened the Norwegian Basin at all time lags (95% significant correlated after 15 months).

4. Discussion

Based on Argo data from 2002 to 2018 in the Norwegian Sea, we presented anomalies of the heat and freshwater content relative to the *WOA18* climatology. Earlier studies have shown that the observed variability during the period 1995–2010 can be attributed to the inflow of warmer and saltier AW to the Norwegian Sea due to circulation changes in the North Atlantic (Häkkinen and Rhines 2004; Hatun et al. 2005) with additional warming due to reduced ocean to air heat loss (Skagseth and Mork 2012). In the recent 2011–18 period, we showed that the warming in the Norwegian Sea continued with about twice as large heat content increase as the previous period, 6.3–7.9 versus 3.2 W m^2 (Skagseth and Mork 2012). However, a different mechanism than in the previous period was responsible for these changes. During the period 2011–18, the covariability between warm/saline and cold/fresh vanished, and instead there has been a period with warming and freshening, and a less dense water mass.

Air–sea interaction processes were proposed by Yashayaev and Seidov (2015) to explain the faster propagation of temperature anomalies compared to salinity anomalies in the Norwegian Sea. While we do not dispute this view in general, this mechanism is likely not the main cause of the recent warming and freshening in the Norwegian Sea. Instead, we find that the recent warming and freshening trend during 2011–18 can be attributed to two mechanisms. First, the inflowing AW in the FSC during 2011–18 became fresher by ~0.1 psu (Hughes et al. 2011; updated to present at http://ocean.ices.dk/iroc/). This may have caused, at least partly, the freshening in the Norwegian and Lofoten Basins in the upper 1000 m by 0.018 and 0.039 psu, respectively, during 2011–18. This is also supported by the fact that the freshening occurred mainly in the upper 400–500 m (Fig. 2), and the degree of lateral exchange between the Norwegian Atlantic Current (NwAC) and the inner basins may also change in time.

Second, as the temperature also decreased simultaneously in the FSC (Hughes et al. 2011; updated to present at http://ocean.ices.dk/iroc/), advection of AW cannot explain the observed warming during 2011–18. During this period, the air–sea heat flux anomaly was on average positive (i.e., less ocean heat loss) in the Norwegian Basin at 4.0 W m^{-2} (Fig. 4a). The observed trend in the heat content in the Norwegian Basin was an increase of 6.3 W m^{-2} for same period (Table 1). Thus, the net local air–sea heat flux could alone explain 63% of the warming of 0.35°C in the upper 1000 m. For comparison, the NCEP air–sea heat flux anomaly gave an average of 3.2 W m^{-2} for the same period. Simultaneously with the warming, the Norwegian Basin freshened in the upper 1000 m by 0.06 m yr^{-1}, a reduction of 0.018 psu over 2011–18, which could be explained by fresher inflowing AW, as mentioned above.

The Lofoten Basin had a similar positive temperature trend as in the Norwegian Basin, 0.05°C yr^{-1}. During 2011–18, the average air–sea heat flux anomaly was also positive in the Lofoten Basin, 2.1 W m^{-2}, but lower than that for the Norwegian Basin. The observed trend in the ocean heat content during 2011–18 gave an average of 7.9 W m^{-2} (Table 1). Thus, the net local air–sea heat flux could alone explain 27% of the Lofoten Basin total warming during 2011–18 (0.39°C) in the upper 1000 m. The lower explained variance for the Lofoten Basin compared to the Norwegian Basin might be the richer eddy fields there (e.g., Koszalka et al. 2011; Poulain et al. 1996), which would influence the estimates. Using the NCEP air–sea heat flux anomaly,

gave 1.7 W m^{-2} for the Lofoten Basin. While the Lofoten Basin had a near similar positive temperature trend as the Norwegian Basin, the freshening trend during 2011–18 was about twice as large compared to that in Norwegian Basin (0.14 vs 0.06 m yr^{-1}). This reduced salinity in the Lofoten Basin of 0.04 psu during 2011–18 could be explained by fresher inflowing water as explained above. The large effect of the freshening in the Lofoten Basin compared to the Norwegian Basin is in accordance with a relatively direct transfer of AW along the Norwegian Atlantic Slope Current before reaching the steep topography in the eastern Lofoten Basin (e.g., Skagseth and Mork 2012).

The local air–sea heat fluxes are important in modifying the ocean heat content in the Norwegian Sea, and this relationship varies with time scales and within basins. In the Norwegian Basin, it became stronger with longer time scales, and from 6 months and higher the air–sea heat fluxes could explain about half the local heat content changes. The lower coherence for the shorter time scales can be related both to larger uncertainty in the Argo-derived estimates (due to relatively less number of profiles; Fig. S2) and to the fact that the hydrography in the Norwegian Basin is also directly influenced by the strength of the NwAC and the EIC, both determined by high-frequency winds (Macrander et al. 2014; Orvik et al. 2001). The low correlation between the ocean heat content and the air–sea heat fluxes when using monthly values can also be explained by the larger uncertainty in the monthly values of the heat content estimates.

In the Lofoten Basin, the coherence estimates were generally higher compared to the Norwegian Sea, especially at high frequencies. The results pointed to differences in how hydrographic anomalies are projected onto the two basins of the Norwegian Sea. The variability in the heat and freshwater content were in the Norwegian Basin mainly limited to the upper 200 m with more high-frequency variability as discussed above. The observed anomalies penetrating deeper in the Lofoten Basin could be related to the deeper mixed layer depth in the Lofoten Basin compared to the Norwegian Basin (Nilsen and Falck 2006).

The importance of the local air–sea heat fluxes on the ocean heat content in the Norwegian Sea are in agreement with Mork et al. (2014). Using yearly hydrographic data, they found that the air–sea heat flux could explain about the half of the interannual variability of the heat content in the Norwegian Sea. In contrast, Carton et al. (2011) used 2-yr smoothed historical hydrographic data from 1950–2009 to conclude that the local air–sea heat flux was too small and instead they argued for advection of anomalies as a more plausible explanation. That they concluded differently might be that they used different temporal resolutions of the data, as 2-yr averages will smooth the interannual variability.

We investigated two possible advective processes responsible for the local residual heat content variability in the Nordic seas: the wind-driven advection of both Atlantic and Arctic water at the FSC and EIC, respectively. Several other processes not investigated herein, such as mesoscale variability, vertical mixing, and so on, may also be of importance. The literature has shown, however, that the two chosen upstream sources are important for the marine climate in the Norwegian Sea (e.g., Blindheim et al. 2000; Helland-Hansen and Nansen 1909). Thus, the focus has been on these two upstream locations.

The short time (monthly to seasonal) response of the stronger wind forcing at both FSC and EIC reduced the heat content and increased the freshwater content in the Norwegian Basin. That southerly wind at FSC decreased the heat content in the Norwegian Basin may seem contradictory, since increased wind speed would increase the NwAC (Skagseth et al. 2004). However, Blindheim et al. (2000) and Mork and Blindheim (2000) used hydrographic observations to show that high winter North Atlantic Oscillation index (i.e., southerly wind) gave a reduced western extension of AW in the Norwegian Basin and, hence, an increased influence of Arctic Water. Connected to this, increased wind-forced advection in the EIC causes larger eastward advection of Arctic Water (Macrander et al. 2014) and thereby cooling the Norwegian Basin.

For the delayed response, we found that the wind at FSC became positive correlated with the ocean heat content in the Norwegian Basin with a time lag of about 1 year. Compatible with these results are the findings of, for example, Chafik et al. (2015) and Holliday et al. (2008), who showed that temperature anomalies take about 1 year to reach the interior Norwegian Sea from the FSC. Broomé and Nilsson (2018) showed that the relatively slow propagation of temperature and salinity anomalies, compared to the faster downstream advection, can be explained by mixing between the boundary current and the interior region of weak mean flow.

Southerly wind at FSC was not significantly correlated with the heat content in the Lofoten Basin. Westerly wind at EIC also reduced the heat content in the upper 1000 m for the Lofoten Basin at seasonal scale. Stronger westerly wind may in this case also lead to an eastward transport of Arctic Water across the Mohns Ridge, from the Greenland Sea to the Lofoten Basin. Increased westerly wind at EIC reduced the heat content also after a 1-yr delay for both the Norwegian

and Lofoten Basins due to advection of Arctic Water. The delayed response can be explained by similar mechanism as mentioned above with anomalies propagating into the Norwegian Sea (Chafik et al. 2015; Holliday et al. 2008).

Thus, the short-term (monthly) response of increased southerly wind reduced the residual ocean heat content due to increased eastward transport of Arctic Water, whereas the long-term (~1 yr) response increased the residual heat content because of increased advection of AW. A similar response, but with opposite sign, was also observed for the freshwater content. On interannual time scales, we expect that the propagation of anomalies becomes more important. Typical propagation speed is $\sim 2\,\mathrm{cm\,s^{-1}}$, and thus they use 1–2 years from the FSC to the Lofoten Basin (e.g., Chafik et al. 2015; Helland-Hansen and Nansen 1909; Holliday et al. 2008). As discussed above, the recent freshening during 2011–18 in the Lofoten Basin was explained by fresher AW being advected into the Norwegian Sea.

It has been reported that the ventilation strength and mixed layer depth in the Greenland Sea can be tied to the properties of AW entering the Norwegian Sea (Latarius and Quadfasel 2016; Lauvset et al. 2018). In a recent study, Lozier et al. (2019) argue that the conversion of warm and salty AW to cold and fresh overflow water in the Nordic seas is largely responsible for the overturning and its variability in the Atlantic. Thus, the observed changes in the AW inflow properties and the modification of AW within the Norwegian Sea may have far-reaching impacts.

5. Conclusions

Ten Argo profiles per month in the Norwegian and Lofoten Basins, respectively, resolved the seasonal hydrographic variation with reasonable accuracy. The comparison between monthly averages of heat and freshwater content with the local air–sea heat flux and the advective processes showed that their influence changed with time scales and time lags. The Argo data also revealed a recent freshening and warming trend in the Norwegian Sea during 2011–18 that could partly be explained by two different mechanisms: reduced ocean heat loss to the atmosphere and advection of fresher AW into the Norwegian Sea. This freshening and warming could further, in a much wider sense, affect the properties of the overflow water that exits the Nordic seas. These results are valuable for model validation and a monitoring framework regarding the predictability of the climate variability in this region.

Acknowledgments. The Argo data were downloaded from the Global Data Assembly Centre in Brest (http://www.coriolis.eu.org/, https:/doi.org/10.17882/42182). These data were collected and made freely available by the International Argo Program and the national programs that contribute to it (http://www.argo.ucsd.edu, http://argo.jcommops.org). The Argo Program is part of the Global Ocean Observing System. The authors are grateful to Ken Drinkwater for the help with the text. Thanks to Anne Sandvik for providing the ERA-Interim dataset (Dee et al. 2011) from the European Centre for Medium-Range Weather Forecasts (ECMWF). NCEP Reanalysis derived data were provided by the NOAA/OAR/ESRL PSD, Boulder, Colorado, USA, from their Web site at https://www.esrl.noaa.gov/psd/. Special thanks to the three anonymous reviewers for their constructive comments and suggestions that improved the paper. This research was supported by the Centre for Climate Dynamics at the Bjerknes Centre for Climate Research through the project AOI.

REFERENCES

Aagaard, K., J. H. Swift, and E. C. Carmack, 1985: Thermohaline circulation in the Arctic Mediterranean Seas. *J. Geophys. Res.*, **90**, 4833–4846, https://doi.org/10.1029/JC090iC03p04833.

Arthun, M., and T. Eldevik, 2016: On anomalous ocean heat transport toward the Arctic and associated climate predictability. *J. Climate*, **29**, 689–704, https://doi.org/10.1175/JCLI-D-15-0448.1.

——, ——, E. Viste, H. Drange, T. Furevik, H. L. Johnson, and N. S. Keenlyside, 2017: Skillful prediction of northern climate provided by the ocean. *Nat. Commun.*, **8**, 15875, https://doi.org/10.1038/ncomms15875.

Blindheim, J., V. Borovkov, B. Hansen, S. A. Malmberg, W. R. Turrell, and S. Østerhus, 2000: Upper layer cooling and freshening in the Norwegian Sea in relation to atmospheric forcing. *Deep-Sea Res. I*, **47**, 655–680, https://doi.org/10.1016/S0967-0637(99)00070-9.

Bosse, A., I. Fer, H. Soiland, and T. Rossby, 2018: Atlantic water transformation along its poleward pathway across the Nordic Seas. *J. Geophys. Res. Oceans*, **123**, 6428–6448, https://doi.org/10.1029/2018JC014147.

Broomé, S., and J. Nilsson, 2018: Shear dispersion and delayed propagation of temperature anomalies along the Norwegian Atlantic Slope Current. *Tellus*, **70A**, 1–13, https://doi.org/10.1080/16000870.2018.1453215.

Carton, J. A., G. A. Chepurin, J. Reagan, and S. Häkkinen, 2011: Interannual to decadal variability of Atlantic Water in the Nordic and adjacent seas. *J. Geophys. Res. Oceans*, **116**, C11035, https://doi.org/10.1029/2011JC007102.

Carval, T., and Coauthors, 2015: Argo user's manual V3.2. Argo Data Management Team, 124 pp., https://doi.org/10.13155/29825.

Chafik, L., J. Nilsson, O. Skagseth, and P. Lundberg, 2015: On the flow of Atlantic water and temperature anomalies in the Nordic Seas toward the Arctic Ocean. *J. Geophys. Res. Oceans*, **120**, 7897–7918, https://doi.org/10.1002/2015JC011012.

Dee, D. P., and Coauthors, 2011: The ERA-Interim reanalysis: Configuration and performance of the data assimilation system. *Quart. J. Roy. Meteor. Soc.*, **137**, 553–597, https://doi.org/10.1002/qj.828.

Eldevik, T., J. E. O. Nilsen, D. Iovino, K. A. Olsson, A. B. Sando, and H. Drange, 2009: Observed sources and variability of Nordic seas overflow. *Nat. Geosci.*, **2**, 406–410, https://doi.org/10.1038/ngeo518.

Emery, W. J., and R. E. Thompson, 1997: *Data Analysis Methods in Physical Oceanography*. Pergamon Press, 634 pp.

Gordon, R. L., and J. M. Huthnance, 1987: Storm-driven continental shelf waves over the Scottish continental shelf. *Cont. Shelf Res.*, **7**, 1015–1048, https://doi.org/10.1016/0278-4343(87)90097-5.

Häkkinen, S., and P. B. Rhines, 2004: Decline of subpolar North Atlantic circulation during the 1990s. *Science*, **304**, 555–559, https://doi.org/10.1126/science.1094917.

Hatun, H., A. B. Sando, H. Drange, B. Hansen, and H. Valdimarsson, 2005: Influence of the Atlantic subpolar gyre on the thermohaline circulation. *Science*, **309**, 1841–1844, https://doi.org/10.1126/science.1114777.

Helland-Hansen, B., and F. Nansen, 1909: *The Norwegian Sea: Its Physical Oceanography Based upon the Norwegian Researches 1900–1904*. Geophysical Institute, University of Bergen, 390 pp.

Holliday, N. P., and Coauthors, 2008: Reversal of the 1960s to 1990s freshening trend in the northeast North Atlantic and Nordic Seas. *Geophys. Res. Lett.*, **35**, L03614, https://doi.org/10.1029/2007GL032675.

Hughes, S. L., N. P. Holliday, and A. Beszczynska-Moller, 2011: ICES report on ocean climate 2010. International Council for the Exploration of the Seas Rep. 309, 69 pp.

Isachsen, P. E., C. Mauritzen, and H. Svendsen, 2007: Dense water formation in the Nordic Seas diagnosed from sea surface buoyancy fluxes. *Deep-Sea Res. I*, **54**, 22–41, https://doi.org/10.1016/j.dsr.2006.09.008.

Kalnay, E., and Coauthors, 1996: The NCEP/NCAR 40-Year Reanalysis Project. *Bull. Amer. Meteor. Soc.*, **77**, 437–471, https://doi.org/10.1175/1520-0477(1996)077<0437:TNYRP>2.0.CO;2.

Koszalka, I., J. H. LaCasce, M. Andersson, K. A. Orvik, and C. Mauritzen, 2011: Surface circulation in the Nordic Seas from clustered drifters. *Deep-Sea Res. I*, **58**, 468–485, https://doi.org/10.1016/j.dsr.2011.01.007.

Langehaug, H. R., D. Matei, T. Eldevik, K. Lohmann, and Y. Gao, 2017: On model differences and skill in predicting sea surface temperature in the Nordic and Barents Seas. *Climate Dyn.*, **48**, 913–933, https://doi.org/10.1007/s00382-016-3118-3.

Latarius, K., and D. Quadfasel, 2016: Water mass transformation in the deep basins of the Nordic Seas: Analyses of heat and freshwater budgets. *Deep-Sea Res. I*, **114**, 23–42, https://doi.org/10.1016/j.dsr.2016.04.012.

Lauvset, S. K., A. Brakstad, K. Våge, A. Olsen, E. Jeansson, and K. A. Mork, 2018: Continued warming, salinification and oxygenation of the Greenland Sea gyre. *Tellus*, **70A**, 1–9, https://doi.org/10.1080/16000870.2018.1476434.

Locarnini, R., and Coauthors, 2019: *Temperature*. Vol. 1, *World Ocean Atlas 2018*, in press.

Lozier, M. S., and Coauthors, 2019: A sea change in our view of overturning in the subpolar North Atlantic. *Science*, **363**, 516–521, https://doi.org/10.1126/science.aau6592.

Macrander, A., H. Valdimarsson, and S. Jónsson, 2014: Improved transport estimate of the East Icelandic Current 2002–2012. *J. Geophys. Res. Oceans*, **119**, 3407–3424, https://doi.org/10.1002/2013JC009517.

Marshall, J., and Coauthors, 2001: North Atlantic climate variability: Phenomena, impacts and mechanisms. *Int. J. Climatol.*, **21**, 1863–1898, https://doi.org/10.1002/joc.693.

Moisan, J. R., and P. P. Niiler, 1998: The seasonal heat budget of the North Pacific: Net heat flux and heat storage rates (1950–1990). *J. Phys. Oceanogr.*, **28**, 401–421, https://doi.org/10.1175/1520-0485(1998)028<0401:TSHBOT>2.0.CO;2.

Mork, K. A., and J. Blindheim, 2000: Variations in the Atlantic inflow to the Nordic Seas, 1955–1996. *Deep-Sea Res. I*, **47**, 1035–1057, https://doi.org/10.1016/S0967-0637(99)00091-6.

——, Ø. Skagseth, V. Ivshin, V. Ozhigin, S. L. Hughes, and H. Valdimarsson, 2014: Advective and atmospheric forced changes in heat and fresh water content in the Norwegian Sea, 1951–2010. *Geophys. Res. Lett.*, **41**, 6221–6228, https://doi.org/10.1002/2014GL061038.

Nilsen, J. E. O., and E. Falck, 2006: Variations of mixed layer properties in the Norwegian Sea for the period 1948–1999. *Prog. Oceanogr.*, **70**, 58–90, https://doi.org/10.1016/j.pocean.2006.03.014.

Orvik, K. A., O. Skagseth, and M. Mork, 2001: Atlantic inflow to the Nordic Seas: Current structure and volume fluxes from moored current meters, VM-ADCP and SeaSoar-CTD observations, 1995–1999. *Deep-Sea Res. I*, **48**, 937–957, https://doi.org/10.1016/S0967-0637(00)00038-8.

Pickart, R. S., and M. A. Spall, 2007: Impact of Labrador Sea convection on the North Atlantic meridional overturning circulation. *J. Phys. Oceanogr.*, **37**, 2207–2227, https://doi.org/10.1175/JPO3178.1.

Poulain, P. M., A. Warn-Varnas, and P. P. Niiler, 1996: Near-surface circulation of the Nordic seas as measured by Lagrangian drifters. *J. Geophys. Res.*, **101**, 18 237–18 258, https://doi.org/10.1029/96JC00506.

Segtnan, O. H., T. Furevik, and A. D. Jenkins, 2011: Heat and freshwater budgets of the Nordic seas computed from atmospheric reanalysis and ocean observations. *J. Geophys. Res. Oceans*, **116**, C11003, https://doi.org/10.1029/2011JC006939.

Sherwin, T. J., S. L. Hughes, W. R. Turrell, B. Hansen, and S. Østerhus, 2008: Wind-driven monthly variations in transport and the flow field in the Faroe-Shetland Channel. *Polar Res.*, **27**, 7–22, https://doi.org/10.1111/j.1751-8369.2007.00036.x.

Skagseth, O., 2004: Monthly to annual variability of the Norwegian Atlantic slope current: connection between the northern North Atlantic and the Norwegian Sea. *Deep-Sea Res. I*, **51**, 349–366, https://doi.org/10.1016/j.dsr.2003.10.014.

——, and K. A. Orvik, 2002: Identifying fluctuations in the Norwegian Atlantic Slope Current by means of empirical orthogonal functions. *Cont. Shelf Res.*, **22**, 547–563, https://doi.org/10.1016/S0278-4343(01)00086-3.

——, and K. A. Mork, 2012: Heat content in the Norwegian Sea, 1995–2010. *ICES J. Mar. Sci.*, **69**, 826–832, https://doi.org/10.1093/icesjms/fss026.

——, K. A. Orvik, and T. Furevik, 2004: Coherent variability of the Norwegian Atlantic Slope Current derived from TOPEX/ERS altimeter data. *Geophys. Res. Lett.*, **31**, L14304, https://doi.org/10.1029/2004GL020057.

Skjoldal, H. R., 2004: *The Norwegian Sea Ecosystem*. Tapir Academic Press, 559 pp.

Søiland, H., and T. Rossby, 2013: On the structure of the Lofoten Basin Eddy. *J. Geophys. Res. Oceans*, **118**, 4201–4212, https://doi.org/10.1002/jgrc.20301.

Swift, J. H., 1984: The circulation of the Denmark Strait and Iceland-Scotland overflow waters in the North Atlantic. *Deep-Sea Res.*, **31A**, 1339–1355, https://doi.org/10.1016/0198-0149(84)90005-0.

Thomson, D. J., 1982: Spectrum estimation and harmonic analysis. *Proc. IEEE*, **70**, 1055–1096, https://doi.org/10.1109/PROC.1982.12433.

Vage, K., and Coauthors, 2011: The Irminger Gyre: Circulation, convection, and interannual variability. *Deep-Sea Res. I*, **58**, 590–614, https://doi.org/10.1016/j.dsr.2011.03.001.

Walczowski, W., J. Piechura, I. Goszczko, and P. Wieczorek, 2012: Changes in Atlantic water properties: An important factor in the European Arctic marine climate. *ICES J. Mar. Sci.*, **69**, 864–869, https://doi.org/10.1093/icesjms/fss068.

Yashayaev, I., and D. Seidov, 2015: The role of the Atlantic Water in multidecadal ocean variability in the Nordic and Barents Seas. *Prog. Oceanogr.*, **132**, 68–127, https://doi.org/10.1016/j.pocean.2014.11.009.

Zweng, M. M., and Coauthors, 2018: *Salinity*. Vol. 2, *World Ocean Atlas 2018*, 40 pp.